Oxidation of Cu_3N thin films obtained from Cu annealed under NH_3:O_2 flow: A Raman and N-K-edge NEXAFS study

Kalliopi Mavridou[a], Matthew Zervos[b], Fani Pinakidou[a], Maria Brzhezinskaya[c], Maria Katsikini[a,*]

[a] School of Physics, Aristotle University of Thessaloniki, GR-54124, Thessaloniki, Greece

[b] Nanostructured Materials and Devices Laboratory, School of Engineering, University of Cyprus, PO Box 20537, Nicosia, 1678, Cyprus

[c] Helmholtz-Zentrum Berlin für Materialien und Energie, Albert-Einstein-Str. 15, 12489 Berlin, Germany

* Corresponding author, e-mail: katsiki@auth.gr, tel: +30 2310998500

Abstract

Cu_3N layers prepared by annealing, under NH_3:O_2 flow, of Cu sputtered on Si, fused SiO_2, and soda-lime-glass were studied by Raman and N-K-edge Near Edge X-ray Absorption Fine Structure (NEXAFS) spectroscopy. The annealing temperatures were ranging from 300 to 800 °C. Benefiting from resonance effects on the Raman peak intensities when different excitation wavelengths are used, the contribution in the Raman signal of copper oxides, which provide peaks lying close to those of Cu_3N, is more easily discriminated. The formation of Cu_2O surface oxide is observed in almost all the samples even for annealing at low temperatures. CuO is generally formed at higher temperatures with the onset depending on the amount of O_2 in the NH_3:O_2 mixture. However, high temperature is necessary to grow larger crystallites, as it is deduced from the decrease in the width of the high-frequency Raman peak (at *ca.* 650 cm^{-1}) of Cu_3N, in accordance with Scanning Electron Microscopy observations. The formation of CuO is accompanied by the creation of N_2 trapped in the sample, which is directly detected by the NEXAFS measurements. N_2 is most probably formed by the N atoms originating from the dissociation of the Cu-N bonds.

1. Introduction

The increasing demand for the combination of lower cost, higher solar energy conversion efficiency and the utilization of non-toxic, earth abundant elements in photovoltaics have led to the development of Cu-based nitrides, such as Cu_3N [1,2]. This semiconductor exhibits a temperature independent direct and indirect band gap of 1.68 and 1.01 eV, respectively, indicating its aptness in solar energy conversion applications [3,4]. Cu_3N crystallizes in the cubic anti-perovskite structure (a = 3.817 Å, space group $Pm\bar{3}m$) with a vacant body-center position which can host many impurities allowing for the control of its p- or n-type character [5-8]. The first attempt to grow Cu_3N involved annealing of CuF_2 under a flow of NH_3 and resulted in the formation of a powder sample [9]. The growth of Cu_3N with a crystallite size in the sub-micrometer scale with ammonolysis of CuF_2 has been also reported [10,11] Recently, Matsuzaki *et al*. [12] developed p- and n- type copper nitride which present high optical absorption coefficient near the direct band gap ($\approx 10^5$ cm^{-1}) and high carrier mobility. Besides photovoltaics, recent studies indicate that Cu_3N thin films are applicable in energy storage [13] and catalysis [14-16] because of their superior chemical activity [17].

Raman spectroscopy is an attractive tool for the fast and non-destructive characterization of semiconductors providing information on their strain state, crystalline quality, and deviations from stoichiometry. The optical phonons, at the center of the Brillouin Zone (Γ point), belong to the irreducible representation $2T_{1u}+T_{2u}$. Although first-order Raman scattering for perfect crystalline Cu_3N is not allowed, Raman modes can be activated in the presence of disorder (e.g., small crystallite size and presence of defects). Raman spectroscopy has been applied for the

study of a Cu-O-N ternary system using green light (λ=514.5 nm) where peaks due to Cu_2O and CuO were detected very close to those of Cu_3N [18]. Green light (λ=532 nm) has also been used for Raman measurements on Cu_xN and it has been found that the position of the T_{1u} mode was ranging from 635 to 610 cm^{-1} for the N/Cu ratio varying from 0.33 to 0.18 [19]. Sahoo and Jain [20] have used red light (λ=632.8 nm) for the study of Cu_3N and detected peaks at 122, 139, 164, 230, 498 and 647 cm^{-1} but they have assigned some of them to oxygen impurities.

One of the most challenging issues in the performance of Cu_3N-based devices is its oxidation. $Cu_2^{(I)}O$ and $Cu^{(II)}O$ are stable and can be formed unintentionally after exposure of the Cu_3N films in air or during the growth as well as intentionally since surface oxides can serve as passivation layers [21,22]. Cu oxides are characterized by optical band gaps in the visible part of the spectrum and exhibit high absorption coefficients [23]. Recent studies state the suitability of Cu_2O thin films (with an optical band gap of 2.17 eV) in heterojunction solar cell applications as active layers, with a theoretical conversion efficiency of 20% [24-27]. Furthermore, the direct band gap of CuO at 1.4 eV renders it an attractive candidate for light-harvesting applications [20,23,28].

Here, we report on the resonance Raman study of Cu_3N layers employing two different laser lines, green and red, with wavelengths, λ, 515.4 and 647.1 nm, in order to discriminate safely the nitride and oxide peaks and discuss the effect of growth conditions on the extent of Cu_3N oxidation and quality. Resonance Raman occurs when the energy of the excitation light is close to that of an electronic, usually an inter-band, transition allowing the selective excitation of different sample

constituents. Furthermore, Near Edge X-ray Absorption Fine Structure (NEXAFS) spectra were recorded at the N-K-edge to investigate alterations in the N-p partial density of states as a function of the growth conditions [29,30].

2. Materials and Methods

Cu films were initially deposited on fused SiO_2 (FS), Si (001) and soda-lime glass (SLG) substrates by sputtering of a Cu target (Aldrich 99.999%) at 10^{-2} mbar under 100% Ar. Similar to Matsuzaki *et al.* [12], Cu was converted to Cu_3N by annealing at temperatures ranging from 300 ºC to 800 ºC under a NH_3:O_2 flow of 150:15 and 300:15 ml/min. The two different gas mixtures are denoted as H (high O_2 percentage) and L (low O_2 percentage), respectively. The growth conditions are summarized in Table S1 (Supplementary Material).

The Raman spectra were recorded using a DILOR XY spectrometer equipped with an optical microscope and a 100× objective. Green (λ= 514.5 nm) and red (λ= 647.1 nm) lines of an Ar^+ and a Kr^+ laser, respectively, were used for the excitation with a power that was less than 2 mW on the sample. The spectra were calibrated utilizing a Ne lamp. The N-K-edge NEXAFS spectra were recorded at the RGBL beamline of the BESSY-II Synchrotron Radiation Facility of the Helmholtz Zentrum Berlin, under ultrahigh vacuum conditions (7×10^{-10} Torr) [31]. The acquisition of the spectra took place in the fluorescence yield (FLY) mode using a QUANTAX QM10 detector. The angle of incidence was 55º to the sample surface providing an information depth of 350 nm, i.e., the entire Cu_3N layer is probed. Total Electron Yield (TEY) spectra were also recorded by measuring the sample's drain current simultaneously with the FLY spectra. The TEY spectra are surface sensitive. Finally, Secondary Electron images

were obtained by a TESCAN Scanning Electron Microscope (SEM) at an accelerating voltage of 30 keV.

3. Results and Discussion

The Raman spectra of two samples grown on Si after annealing of Cu at 400 ºC and 600 ºC (NH_3:O_2 300:15 ml/min) are shown in Figs. 1(a) and (b), respectively. Peaks assigned to Cu oxides contribute strongly revealing that oxidation of Cu_3N occurs. The peak positions of Cu_2O and CuO phases determined in the case of Cu layers deposited on FS that were subjected to annealing under different conditions are included in the Supplementary Material [20,32-37]. Differences in the CuO peak positions included in the Supplementary Material from those marked in Fig. 1, are attributed to size effects [38]. As it is evident from Fig. 1, in the spectra of the Cu_3N sample prepared after annealing at 400 ºC only the Cu_2O oxide is present. When annealing is performed at higher temperatures, CuO is also detected. Due to the different electron energy band gaps of Cu_3N, Cu_2O and CuO, resonance effects are expected to occur by varying the wavelength of the laser beam. A comparison of the corresponding energies is shown in the inset of Fig. 1(a). When light with λ=514.5 nm (2.41 eV) is used, resonance effects are expected for Cu_2O [39,40]. It is a direct band gap semiconductor but the transitions from the top of the valence band to the bottom of the conduction band are parity forbidden. Transitions between the split valence bands and the second lowest conduction band are direct and allowed, resulting in strong absorption at approximately 2.6-2.7 eV [41,42]. On the other hand, the signal of Cu_3N is expected to be low due to the forbidden character of the lattice vibrations. However, for λ=647.1 nm, the Cu_3N signal is enhanced in comparison to that of Cu_2O. Therefore, under these conditions, the bands at 170 (T_{2u}) and 655 (T_{1u})

have to be assigned to Cu_3N. Furthermore, it should be also mentioned that the peak at *ca.* 521 cm^{-1} originating from the Si substrate is more pronounced in the spectrum recorded with λ=647.1 nm. This observation can be explained by the low absorption (at this energy the surface Cu_2O layer does not absorb) that results in larger information depth.

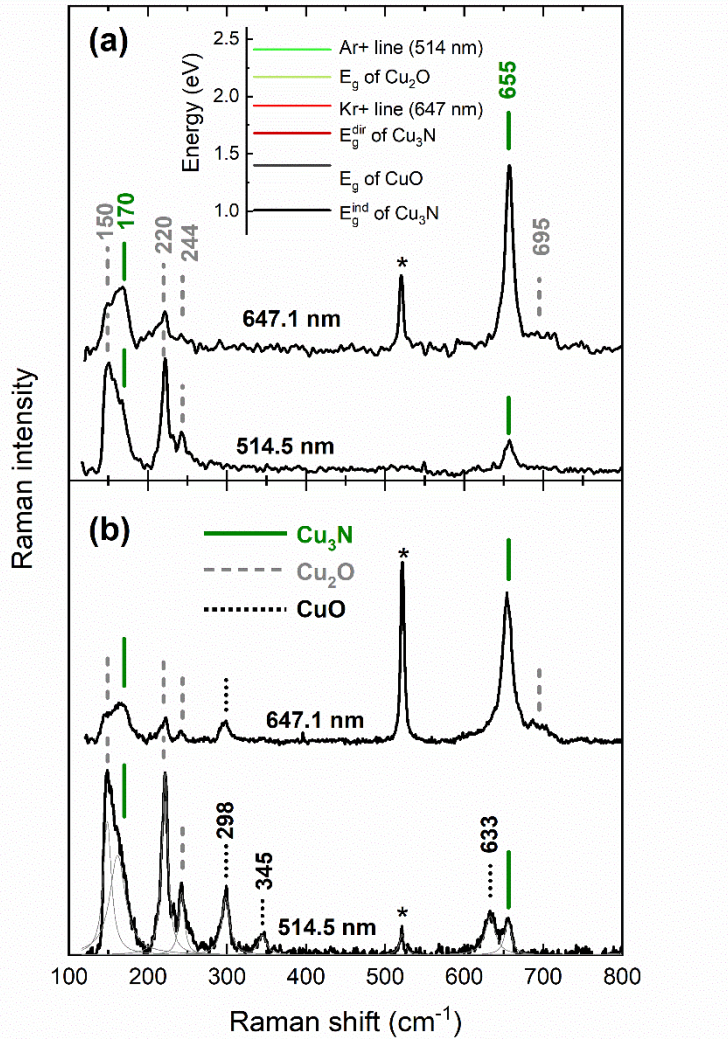

Figure 1 (color online): Raman spectra of Cu_3N samples prepared after annealing of Cu under 300:15 ml/min NH_3:O_2 gas flow at **(a)** 400 ºC, L1, and **(b)** 600 ºC, L5, recorded using two different laser lines. Solid green, dashed grey, and dotted black vertical lines indicate the Cu_3N, Cu_2O and CuO peak positions, respectively. An energy diagram that compares the band gap energy levels with the light energy used for the excitation, is shown in the inset of (a). The peak marked by an asterisk

corresponds to the Si substrate. Representative fitting using Lorentz lineshapes plotted in thin grey lines, is shown in the bottom of (b). The Raman spectra were subjected to subtraction of a smooth background.

The fitting results for the samples annealed under the high O_2 content in the NH_3:O_2 gas mixture, indicate that the position, ω, of the T_{1u} peak shifts to higher energies with annealing temperature, as shown in Fig. 2(a). The positions of the Cu_3N peaks, especially of the T_{1u} peak, are sensitive to strain, stoichiometry and presence of defects or oxygen [19,43,44]. Moreover, the Full Width at Half Maximum (FWHM) of the same peak decreases with the annealing temperature [Fig. 2(b)] designating the increase in the crystallite size. The results lie in agreement with the SEM observations presented in Fig. 2(c)-(e), where it is obvious that the crystallite size increases as the annealing temperature rises from 400 to 600 ºC. The increase in the crystallite size is expected to have beneficial effects on the carrier transport as the scattering probability of the electrons by the boundaries is reduced.

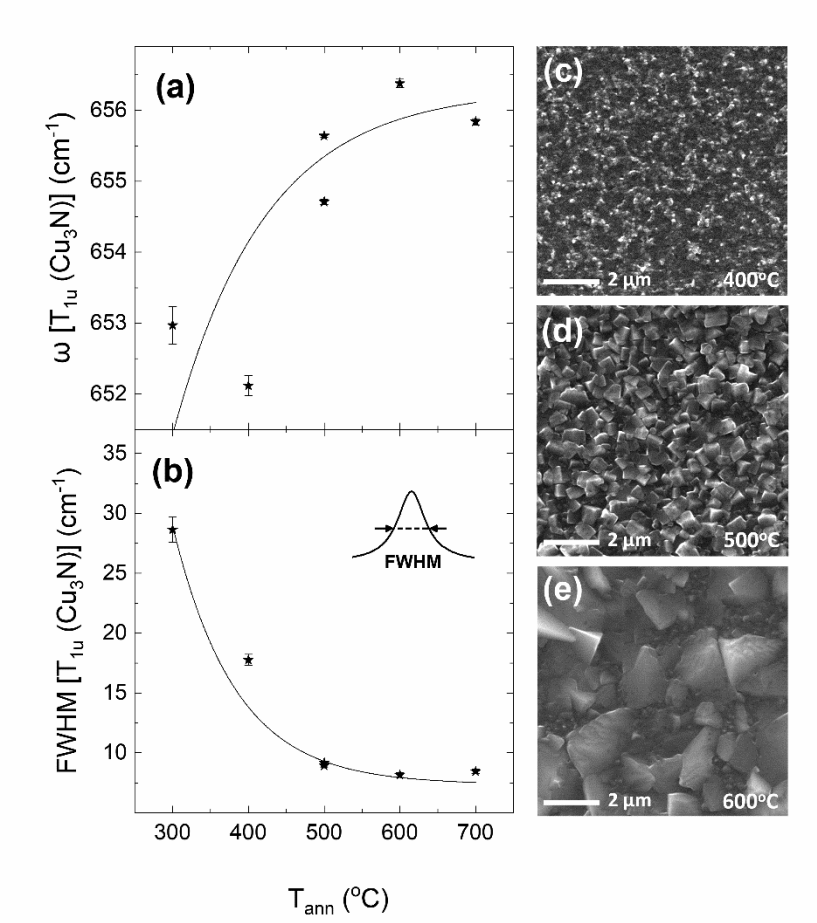

Figure 2: (a) Position, ω, and **(b)** FWHM of the T_{1u} peak of Cu_3N samples annealed under 150:15 mL/min NH_3:O_2 flow as a function of the annealing temperature. Secondary electron SEM images of the samples annealed at **(c)** 400, **(d)** 500 and **(e)** 600 ºC.

Although the desired increase in the crystallite size can be achieved by annealing at higher temperatures, the latter promotes the formation of oxides. In order to investigate the extent of oxidation of the Cu_3N films, the relative intensity (defined as the peak area) of Raman peaks that correspond to CuO or Cu_2O and Cu_3N was determined. In Fig. 3(a) the intensity ratios of the T_{1u}^{l} peak of Cu_2O (~150 cm^{-1}) and the A_g peak of CuO (~295 cm^{-1}) with the T_{2u} peak of Cu_3N (~170 cm^{-1}), are plotted as a function of the annealing temperature. The results correspond to the spectra recorded with λ=647.1 nm because they provide larger information depth and better

discrimination of the Cu_3N peaks due to resonance effects. It is evident that the Cu_2O phase can be more easily developed, even from 300°C. However, increase in the annealing temperature results in increase in the Cu_2O content of the sample, most probably on its surface since its peaks are easily detected using both the green and red laser light. Figs. 3(b) and 3(c) show the corresponding ratios for the samples annealed with low O_2 content of the gas mixture. The layers of this sample series were grown on different substrates and are of various thicknesses. The CuO phase is mainly detected for annealing temperatures higher than 500°C and its formation is enhanced as the annealing temperature increases. When the NH_3:O_2 mixture with high O_2 content is used, the extent of oxidation is greater. It should be noted that the formation of the Cu_3N phase was also verified by X-ray Diffraction (XRD) (see Supplementary Material). Spectra recorded from samples grown on different substrates at the same temperature and under the same gas flow are also included in the Supplementary Material.

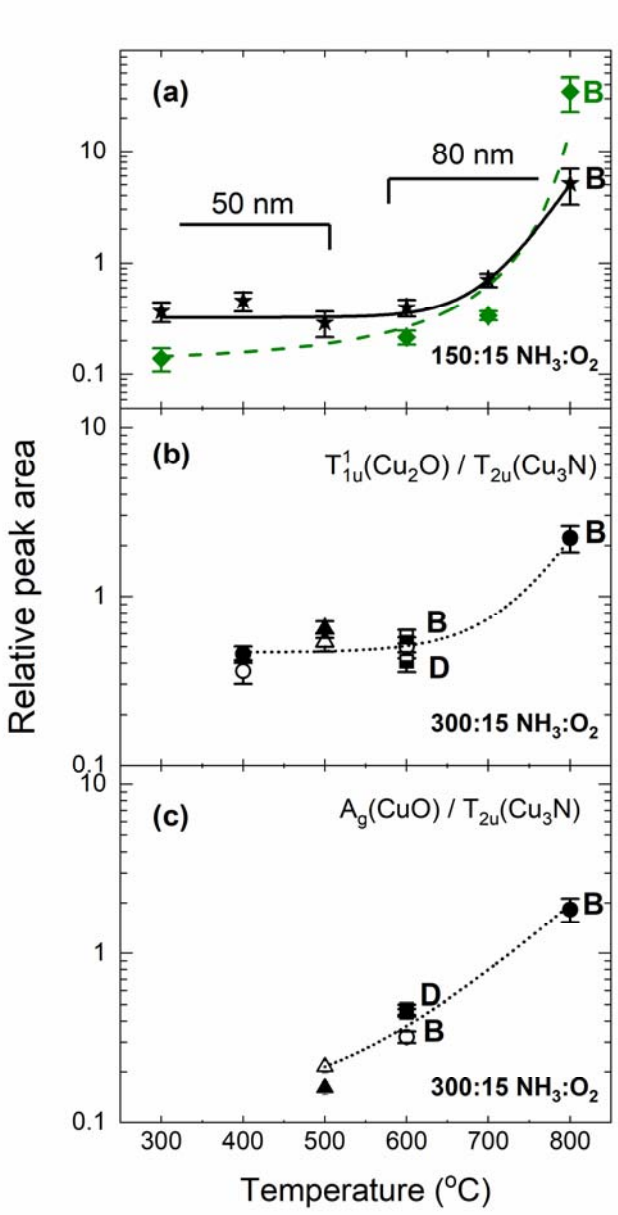

Figure 3 (color online): (a) Relative peak areas as a function of annealing temperature for the samples annealed under a NH_3:O_2 flow with high O_2 content. Black stars and green rhombuses correspond to the $T^1_{1u}(Cu_2O)/T_{2u}(Cu_3N)$ and $A_g(CuO)/T_{2u}(Cu_3N)$ ratios, respectively. **(b,c)** $T^1_{1u}(Cu_2O)/T_{2u}(Cu_3N)$ and $A_g(CuO)/T_{2u}(Cu_3N)$ peak area ratios as a function of annealing temperature for the samples annealed under a NH_3:O_2 flow with low O_2 content. Circles, triangles, and squares correspond to layers grown on Si, SLG and FS substrates, respectively. Empty, half-filled, and filled symbols correspond to 30, 60, and 120 nm-thick layers, respectively. B and D refer to spectra recorded from sample regions that appear bright or dark using the microscope attached on the Raman setup, respectively. The results

correspond to the spectra recorded with λ=647.1 nm. The error bars refer to the standard error of the fitting process. The lines are guides to the eye.

Fig. 4(a) shows the N-K-edge NEXAFS spectra of the samples grown on Si annealed at different temperatures under NH_3:O_2 flow with high O_2 content. The NEXAFS spectra are proportional to the N-p partial density of empty states, exhibiting maxima denoted as a-d. Annealing up to 600 ºC does not induce changes in the spectra. However, annealing at 800 ºC causes detrimental alterations with a dominant peak appearing at *ca.* 402 eV. The high-resolution spectrum shown in Fig. 4(b) reveals the hyperfine structure of this peak which can be fitted with a number of equidistant Lorentzian functions. This behavior is characteristic of the vibronic transitions of N_2, which refer to transitions where both the electronic and the vibrational states change [30]. The same hyperfine structure is also observed in the spectrum of the sample annealed at 700 ºC. However, in this case the N_2 peak is superimposed on peak b of Cu_3N. Therefore, it can be proposed that the oxidation of Cu_3N is accompanied by the formation of molecular nitrogen. It should be pointed out, that the spectra recorded with the surface sensitive electron yield mode, using the sample photocurrent, were identical to the bulk sensitive fluorescence yield spectra. This is an indication that the formation of N_2 takes place throughout the sample. It has been reported that denitridation of Cu_3N takes place after annealing under Ar:H_2 flow where up to 30 % of N is reduced towards the formation of NH_3. The elimination of N_2 has been resulted in the formation of pores [45]. The increased porosity may lead to enhanced performance of lithium metal batteries [46].

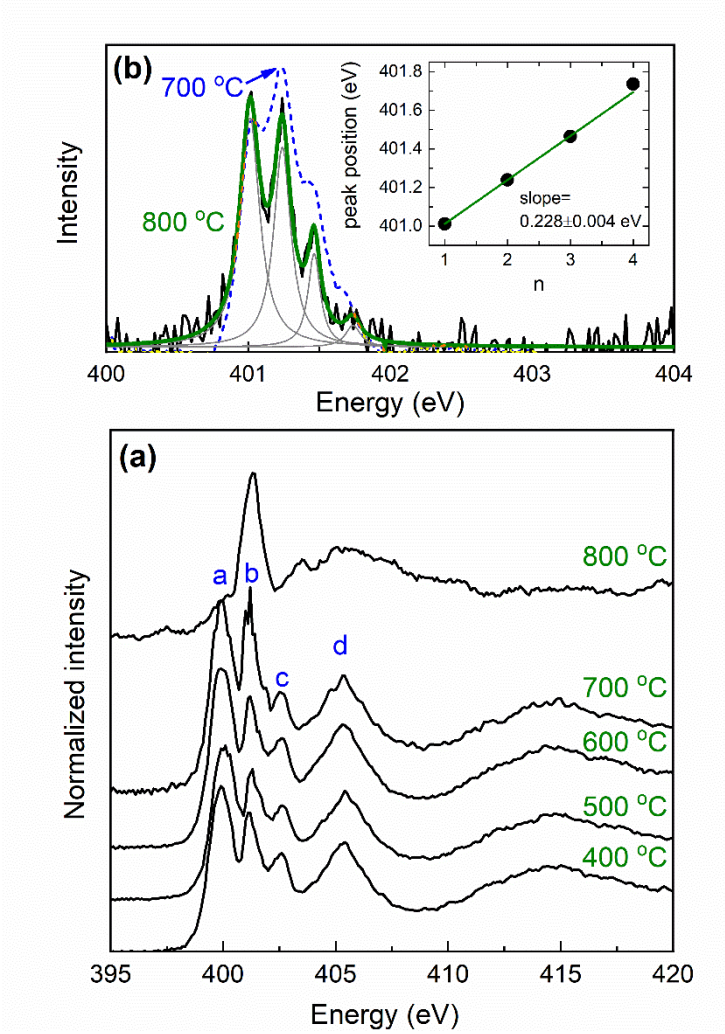

Figure 4 (color online): (a) N-K-edge NEXAFS spectra of the Cu_3N layers grown on Si after annealing at temperatures ranging from 400 to 800 ºC under NH_3:O_2 (150:15 mL/min). **(b)** High-Resolution spectra recorded around the peak b and fitting with Lorentzian lineshapes. The inset indicates that the Lorentzians are equidistant.

The formation of Cu_2O and CuO could be attributed to the exposure of the Cu_3N layer in air [22], to oxygen diffusion from the substrate at elevated temperatures (even from the native oxide formed on the Si surface), and/or to the oxygen used in the growth procedure. The formation of Cu_2O on the surface of Cu_3N left in air has been attributed to substitution of N by O atoms [47]. On the other hand, the growth

procedure appears to play a dominant role since the extent of oxidation and the threshold temperature for oxide formation are affected by the O_2 percentage in the annealing gas mixture (see Fig. 3). The growth route adopted here is the one proposed by Matsuzaki *et al.* [12], according to which the introduction of O_2 into the NH_3 gas during annealing assists the N-H cleavage promoting the Cu nitridation. More specifically, an O_2 molecule that is adsorbed on the Cu metal surface is transformed to an oxygen species (such as O_2^-) that selectively oxidizes a NH_3 molecule (dehydrogenation) to form NH_2 and NH transient products, which create nitrogen adatoms on the surface that immediately migrate into the bulk forming Cu_3N. In this context, the annealing temperature might affect the oxide formation in two ways: it can cause dissociation of the Cu-N bonds and subsequent formation of Cu-O bonds [20,48] or it may promote the decomposition of NH_x transient species towards the formation of N_2. The formation of N_2 for annealing temperatures ≥700 ºC is directly detected by the N-K-edge NEXAFS measurements, revealing that N_2 is trapped in the Cu_3N films. In the sample annealed at 800 ºC, molecular nitrogen is the dominant N species detected. N_2 is expected to be formed on the sample surface after the decomposition of NH_3. However, our results suggest that the detected N_2 is formed throughout the film after the combination of atomic nitrogen originating from the dissociation of the Cu-N bonds at high annealing temperatures. Based on the Raman results, which demonstrate that both the annealing temperature and the O_2 content in the NH_3:O_2 mixture affect the growth process, the growth procedure can be further optimized.

4. Conclusions

In conclusion, Cu_3N thin films were prepared by annealing of Cu in a NH_3:O_2 atmosphere. The samples were studied by means of Raman and N-K-edge NEXAFS spectroscopies. Resonance effects were employed to enhance the Cu_3N contribution in the Raman spectra with the red line of a Kr^+ laser (λ=647.1 nm) being more efficient for the detection of Cu_3N compared to the green line of an Ar^+ laser (λ=514.5 nm). The Raman spectra revealed the presence of a surface Cu_2O phase in almost all the films grown after annealing of Cu at various temperatures and under two different NH_3:O_2 mixtures. For a series of samples grown on Si, it was found that the annealing temperature controls the grain size. Irrespective of the type of the substrate and the O_2 content of the NH_3:O_2 gas mixture, elevated temperatures were found to cause the formation of CuO. The extent of both the Cu_2O and CuO formation depends on both the annealing temperature and the O_2 percentage of the NH_3:O_2 gas mixture. The presence of CuO is accompanied by the formation of N_2 trapped in the Cu_3N film, as it is directly detected by the NEXAFS measurements. Therefore, the proposed mechanism of CuO growth as well as the enhancement of Cu_2O contribution as the annealing temperature increases, is the Cu-N bond dissociation that occurs throughout the film leading to the formation of N_2 and Cu-O bonds with the oxygen atoms available in the NH_3:O_2 gas mixture. As high temperatures are necessary to grow larger crystallites towards better carrier transport, this cost effective and simple growth method should be further optimized.

Acknowledgements

The measurements at BESSY-II were funded by the European Union's Horizon 2020 research and innovation programme under grant agreement No 730872 (CALIPSOplus). The support of Dmitry Smirnov during the measurements at RGBL is greatly acknowledged. We thank Helmholtz-Zentrum Berlin (HZB) for the allocation of synchrotron radiation beamtime.

Supplementary material

See supplementary material for additional information on the samples, the peak positions of the copper oxide phases, and the effect of substrate.

References

[1] S. C. Chen, S. Y. Huang, S. Sakalley, A. Paliwal, Y. H. Chen, M. H. Liao, H. Sun, S. Biring, J. Alloys Compd. 789 (2019) 428-434.

[2] K. Matsuzaki, T. Okazaki, Y. S. Lee, H. Hosono, T. Susaki, Appl. Phys. Lett. 105 (2014) 222102.

[3] M. Birkett, C. N. Savory, A. N. Fioretti, P. Thompson, C. A. Muryn, A. D. Weerakkody, I. Z. Mitrovic, S. Hall, R. Treharne, V. R. Dhanak, D. O. Scanlon, A. Zakutayev, T. D. Veal, Phys. Rev. B 95 (2017) 115201.

[4] M. Sergides, M. Zervos, A. Othonos, J. Appl. Phys. 128 (2020) 125704.

[5] D. Barman, S. Paul, S. Ghosh, S. K. De, ACS Appl. Nano Mater. 2 (2019) 5009.

[6] L.-C. Wang, B.-H. Liu, C.-Y. Su, W.-S. Liu, C.-C. Kei, K.-W. Wang, T.-P. Perng, ACS Appl. Nano Mater. 1 (2018) 3673.

[7] M. Zervos, A. Othonos, M. Sergides, T. Pavloudis, J. Kioseoglou, J. Phys. Chem. C 124 (2020) 3459.

[8] W. Yu, J. Zhao, C. Jin, Phys. Rev. B 72 (2005) 214116.

[9] R. Juza and H. Hahn, Zeitschrift für anorganische und allgemeine Chemie, 239 (1938) 282.

[10] X. Li, A. Hector and J. Owen, The Journal of Physical Chemistry C, 118 (2014) 29568.

[11] G. Paniconi, Z. Stoeva, H. Doberstein, R. I. Smith, B. L. Gallagher, and D. H. Gregory, Solid State Sciences 9 (2007) 907.

[12] K. Matsuzaki, K. Harada, Y. Kumagai, S. Koshiya, K. Kimoto, S. Ueda, M. Sasase, A. Maeda, T. Susaki, M. Kitano, F. Oba, H. Hosono, Adv. Mater. 30 (2018) 1801968.

[13] J. Wang, F. Li, X. Liu, H. Zhou, X. Shao, Y. Qu, M. Zhao, J. Mater. Chem. A 5 (2017) 8762.

[14] Z. Wang, X. Cao, D. Liu, S. Hao, R. Kong, G. Du, A.M. Asiri, X. Sun, Chem. - Eur. J. 23 (2017) 4986.

[15] C. Panda, P.W. Menezes, M. Zheng, S. Orthmann, M. Driess, ACS Energy Lett. 4 (2019) 747.

[16] Z. Yin, C. Yu, Z. Zhao, X. Guo, M. Shen, N. Li, M. Muzzio, J. Li, H. Liu, H. Lin, J. Yin, G. Lu, D. Su, S. Sun, Nano Lett. 19 (2019) 8658.

[17] A. Jiang, M. Qi, J. Xiao, J. Mater. Sci. Technol. 34, (2018) 1467.

[18] A. Fallberg, M. Ottosson, J.-O. Carlsson, J. Cryst. Growth 312 (2010) 1779.

[19] K. Nowakowska-Langier, R. Chodun, R. Minikayev, S. Okrasa, G. W. Strzelecki, B. Wicher, K. Zdunek, J. Mol. Struct. 1165 (2018) 79.

[20] G. Sahoo, M. K. Jain, Appl. Phys. A: Mater. Sci. Process. 118 (2015) 1059.

[21] V.-H. Castrejón-Sánchez, A. C. Solís, R. López, C. Encarnación-Gomez, F. M. Morales, O. S. Vargas, J. E. Mastache-Mastache, G.V. Sánchez, Mater. Res. Express 6 (2019) 075909.

[22] A. Zakutayev, C. M. Caskey, A. N. Fioretti, D. S. Ginley, J. Vidal, V. Stevanovic, E. Tea, S. Lany, J. Phys. Chem. Lett. 5 (2014) 1117.

[23] B. K. Meyer, A. Polity, D. Reppin, M. Becker, P. Hering, B. Kramm, P. J. Klar, T. Sander, C. Reindl, C. Heiliger, M. Heinemann, C. Müller, C. Ronning, Semicond. Semimetals 88 (2013) 201–226.

[24] J. Su, Y. Zhang, L. Liu, R. Sun, Q. Niu, Thin Solid Films 651 (2018) 67.

[25] A. S. Zoolfakar, R. A. Rani, A. J. Morfa, A. P. O'Mullane, K. Kalantar-zadeh, J. Mater. Chem. C 2 (2014) 5247.

[26] S. Boudour, I. Bouchama, M. Hadjab, S. Laidoudi, Opt. Mater. 98 (2019) 109433.

[27] W. Ismail, N.M. El-Shafai, A. El-Shaer, M. Abdelfatah, Mater. Sci. Semicond. Process. 120 (2020) 105335.

[28] N. R. Dhineshbabu, V. Rajendran, N. Nithyavathy, R. Vetumperumal, Appl. Nanosci. 6 (2016) 933.

[29] M. Katsikini, E. C. Paloura, and T. D. Moustakas, Appl. Phys. Lett. 69 (1996) 4206.

[30] M. Katsikini, F. Pinakidou, E. C. Paloura, E. Wendler, W. Wesch, R. Manzke, J. Phys.: Conf. Ser. 190 (2009) 012065.

[31] S. L. Molodtsov, S. I. Fedoseenko, D. V. Vyalikh, I. E. Iossifov, R. Follath, S. A. Gorovikov, M. M. Brzhezinskaya, Y. S. Dedkov, R. Püttner, J.-S. Schmidt, V. K. Adamchuk, W. Gudat, G. Kaindl, Appl. Phys. A : Mater. Sci. Process. 94 (2008) 501.

[32] A. Anu, M. Abdul Khadar, AIP Adv. 5 (2015) 097176.

[33] T.H. Tran, V.T. Nguyen, Int. Sch. Res. Notices 2014 (2014) 1.

[34] Y. Deng, A. D. Handoko, Y. Du, S. Xi, B. S. Yeo, ACS Catal. 6 (2016) 2473.

[35] L. Debbichi, M.C. Marco de Lucas, J.F. Pierson, P. Krüger, J. Phys. Chem. C 116 (2012) 10232.

[36] D. Powell, A. Compaan, J. R. Macdonald, Phys. Rev. B 12 (1975) 20.

[37] T. Sander, C. T. Reindl, M. Giar, B. Eifert, M. Heinemann, C. Heiliger, P. J. Klar, Phys. Rev. B 90 (2014) 045203.

[38] P. S. Murthy, V. P. Venugopalan, D. A. Das, S. Dhara, R. Pandiyan, and A. K. Tyagi, *International Conference on Nanoscience, Engineering and Technology* (ICONSET 2011) (IEEE, 2011).

[39] N. A. M. Shanid, M. A. Khadar, V. G. Sathec, J. Raman Spectrosc. 42 (2011) 1769.

[40] P. Y. Yu, Y. R. Shen, Y. Petroff, Solid State Commun. 12 (1973) 973.

[41] H. Amekura, N. Kishimoto. Fabrication of Oxide Nanoparticles by Ion Implantation and Thermal Oxidation. Toward Functional Nanomaterials, Springer, New York, 2009, pp. 1-75.

[42] M. Cheon, B. Jung, S. J. Kim, J. I. Jang, S. Y. Jeong, J. Alloys Compd. 801 (2019) 536.

[43] M. Zervos, A. Othonos, T. Pavloudis, S. Giaremis, J. Kioseoglou, K. Mavridou, M. Katsikini, F. Pinakidou, E. C. Paloura, J. Phys. Chem. C 125 (2021) 3680.

[44] M. Wilczopolska, K. Nowakowska-Langier, S. Okrasa, L. Skowronski, R. Minikayev, G. W. Strzelecki, R. Chodun, K. Zdunek, Materials 14 (2021) 2694.

[45] A.-M. Alexander, J. S. J. Hargreaves, and C. Mitchell, Top Catal. 55 (2012) 1046.

[46] M. Zhao, X. Huang, D. Zhuang, L. Sheng, X. Xie, M. Cao, J. Pan, H. Fan and J. He, Journal of Energy Storage, 47 (2022) 103665.

[47] D. Dorranian, L. Dejam, Mol. Cryst. Liq. Cryst. 575 (2013) 49.

[48] T. Maruyama, T. Morishita, J. Appl. Phys. 78 (1995) 4104.